Design of a Solid Freeform Fabrication Diamond Reactor

W. Richards Thissell,[1,2] James Tompkins,[2] and Harris L. Marcus[1,2]

1. Department of Mechanical Engineering
2. Center for Materials Science and Engineering
ETC 9.104
University of Texas at Austin
Austin, Texas 78712
(512) 471-1504
FAX: (512) 471-7681

Abstract

Solid Freeform Fabrication (SFF) has progressed from the visualization aided stage of computer aided designs (CAD) to rapid prototyping of structural parts. Among the promising techniques for producing structural prototypes is the technology of chemical vapor deposition (CVD) of polycrystalline diamond. This paper discusses the thermodynamic and kinetic theories that suggest that structural diamond may be rapidly deposited at rates approaching 1 mm/hr from the vapor phase at metastable thermodynamic conditions. The design of a reactor that will produce structural diamond prototypes is discussed. This reactor combines downstream microwave plasma enhanced chemical vapor deposition (DMWPECVD) with a scanned CO_2 laser that locally heats the substrate to diamond deposition temperatures. The input gases are H_2, O_2, CH_4, and Ar. The operating pressure range of the reactor is 1×10^{-2} to 7×10^{2} Torr. The reactor is designed for *in situ* determination of deposit thickness while deposition occurs as well as having the capacity of fitting on an existing resonance enhanced multiphoton ionization time of flight mass spectroscopy (REMPITOFMS) apparatus that will allow for plasma diagnostics immediately above the heated substrate. Plasma diagnostics will be employed to determine the active metastable species that results in diamond deposition so that optimization can be made of the operating parameters to maximize diamond selectivity and deposition rate.

1 Table of Symbols

A	Degree of Absorption, Dimensionless
$C_{A,B,...D}$	Concentration of Species A,B,...D, $\frac{\text{moles}}{\text{cm}^3}$
C_p	Constant Pressure Heat Capacity, $\frac{\text{J}}{\text{gK}}$
D	Diffusion Coefficient of Binary Mixture, $\frac{\text{m}^2}{\text{sec}}$
E_i	Activation Energy, $\frac{\text{KJ}}{\text{mol}}$
ΔE_i	Photolytic Activation Energy, $\frac{\text{KJ}}{\text{mol}}$
H	Enthalpy, $\frac{\text{KJ}}{\text{mole}}$
I, I_o, I_1	Light Source Intensity, $\frac{\text{W}}{\text{cm}^2}$
$\mathbf{J}^*$	Mass Flux Relative To The Molar Average Velocity, $\frac{\text{moles}}{\text{m}^2\text{sec}}$
K	Thermal Conductivity, $\frac{\text{W}}{\text{mK}}$
K	Equilibrium Constant, moles$^{\frac{\Sigma(n,o,\ldots,z)}{\Sigma(a,b,\ldots,m)}}$
M	Molar Mass, $\frac{\text{kg}}{\text{mole}}$
P_i^{sat}	Vapor Pressure of species i, Pa
P_i	Partial Pressure of species i, Pa
P_o	System Pressure, Pa
${}^{i_s}P_{i_g}^{\circ}$	Equilibrium Vapor Pressure of species i_g over i_s, ${}^{i_s}P_{i_g}^{\circ} = f(T)$, Pa
R	Gas Constant, $\frac{\text{KJ}}{\text{mol K}}$
R_i	Reaction Rate, $\frac{\text{moles}}{\text{cm}^3\,\text{sec}}$
T	Temperature, °K
T_{lv}	Boiling Point, °K
T_{sl}	Melting Point, °K
c	Total Molar Concentration, $\frac{\text{moles}}{\text{m}^3}$
c_A	Molar Concentration of Species A, $\frac{\text{moles}}{\text{m}^3}$
d	Diameter of Reaction Zone, m
j_m	Molar Flux of Melt Relative To Stationary Coordinates, $\frac{\text{moles}}{\text{m}^2\,\text{sec}}$
k_i	Reaction Rate Constant, $\frac{\left(\frac{\text{mol}}{\text{cm}^3}\right)^{1-n}}{\text{sec}}$
n	Total Reaction Rate Order, $n = \sum_i n_i$, Dimensionless
$n_{a,b,...f}$	Reaction Rate Concentration Power Dependencies, Dimensionless
r_f	Focus Radius, m
t	Time, sec
v	Velocity, $\frac{\text{m}}{\text{sec}}$
v_m	RMS Velocity of Reactant Molecules Near The Surface, $\frac{\text{m}}{\text{sec}}$
Λ	Mean Free Path, m

α	Thermal Diffusivity, $\frac{K}{\rho C_p}, \frac{m^2}{sec}$
γ_i	Net Rate of Change of species i, sec^{-1}
η'	Sticking Coefficient, Dimensionless
κ	Boltzmann Constant, $\kappa = 1.380 \times 10^{-23} \frac{J}{K}$
λ	Wavelength, m
μ	Viscosity, Pa sec
ρ_i	Density of species i, $\frac{kg}{m^3}$
σ	A Lennard-Jones Parameter, Å
τ_o	Time Required To Approach Steady State, sec
υ	Fuller, Schettler, and Gidings Diffusion Volume Increments

2 History of Vapor Phase Diamond Synthesis

Deposition of solid material from selected gases has great potential as an alternative freeform fabrication technique. The use of reactant gases (or precursors) in a chemical reactor to grow layers of a desired material is commonly known as Chemical Vapor Deposition (CVD), and is widely used on a commercial scale. An exciting and unique application of this concept is used below to propose the freeform fabrication of diamond from gas phase hydrocarbons.

Diamond growth from the gas phase for freeform fabrication is complicated by factors not encountered in normal chemical vapor deposition. First, diamond is a metastable phase at all reasonable temperatures and pressures. Under most conditions, carbon will be deposited having the equilibrium *sp2* bonding. However, under kinetically controlled conditions,[1] some carbon is deposited in the metastable *sp3* bonded state. The activation energy needed for diamond to transform to the more stable graphite structure is quite high at $730 \pm 50 \frac{kJ}{mol}$ for {110} planes,[2] making diamond quite stable at temperatures below 1600 °C in oxygen partial pressures less than 10^{-6} Torr. The removal of *sp2* bonded carbon may be accomplished during growth by using a high percentage of atomic hydrogen in the gas phase, which preferentially etches *sp2* bonded carbon over *sp3* bonded carbon.[3] Furthermore, hydrogen stabilizes the dangling *sp3* bonds present at the surface of the diamond layer and prevents them from collapsing into a *sp2* bonded surface structure.

The first reported growth of diamond from the gas phase was from von Bolton in Germany (1911), using acetylene and mercury at 100 °C.[4] Simple acetylene torches were used in Germany by researchers beginning in the 1940's.[5] The first documented work confirmed by others was by Eversole of Union Carbide in 1952.[6] It is interesting to note that this is two years earlier than the first diamond synthesis by the well known high pressure method developed by General Electric in 1954.[7] In 1956, a patent was filed in the Soviet Union by Deryagin and Fedoseev for the growth of diamond from carbon containing gases.[8] Both Eversole and Deryagin deposited graphite and diamond simultaneously on the substrate, then preferentially etched away the graphite with oxygen or high pressure hydrogen to give a small net gain of diamond. In 1966, Lander and Morrison of Bell Telephone Laboratories discovered the importance of a hydrogen-rich environment in preventing the conversion of the diamond surface to graphite due to unsatisfied *sp3* bonds.[9] Later, Angus from Case Western Reserve University used this information and Eversole's hydrogen etching to alternately grow and clean diamond films.[10] He also increased the growth rate by using a methane and hydrogen gas mixture. Finally, Vickery of Diamond Squared Industries combined the growth and etching cycles into a continuous, single step process by using 95% hydrogen and 5% hydrocarbon (1978).[11]

The key to rapid, continuous film growth was provided by Deryagin. His identification of atomic hydrogen as a rapid graphite scavenger dictated the design of all subsequent diamond growth chambers. He describes[12] five methods of generating a stable source of atomic hydrogen - catalysis, ion beam, electron beam, heated filament, and plasma excitation, the latter two of which are used on nearly all modern reactors. Deryagin also demonstrated continuous diamond film growth on a non-diamond substrate, a milestone in the pursuit of a commercially viable process.

In 1974, scientists from Japan's National Institute for Research in Inorganic Materials (NIRIM) began work on diamond deposition from the gas phase. Using the heated filament method above, they produced films more suitable for commercial use. Later, plasma based methods made their coatings easier to produce and more consistent in quality.[13] Japan now holds by far the largest number of patents (over 500) on commercial diamond films, and there are many coordinated industrial groups actively pursuing research.

3 Diamond Characterization and Classification

Carbon may bond by several different hybridized orbitals, *sp1*, *sp2*, and *sp3*. Carbon may be amorphous, having either *sp* bonded carbon (carbyne), *sp2* bonded carbon, or *sp3* bonded carbon. Carbon may have a hexagonal lattice with space group $P6_3/mmc$ and $P6_3mc$ for *sp2* bonded carbon, a hexagonal *sp3* bonded lattice with space group $P6_3/mmc$ (londaleite), and a diamond *sp3* bonded crystal lattice with space group $Fd3m$. Carbon solids may also be formed with combinations of two or more of the above lattice types. Diffraction data for all of the above lattices and space groups may be very similar and easily misinterpreted. Raman spectroscopy has proven to be the best technique for characterization of carbon solids. The Raman spectra does not directly provide information about the crystal structure, only the electronic state of the bonding. However, pure graphite consists of only *sp2* bonding and that pure diamond consists of only *sp3* bonding and that amorphous carbons may consist of both *sp2* and *sp3* bonding.

The Raman spectrum of hexagonal graphite consists of a single narrow peak at 1580 cm^{-1}, and weak lines at 2450 cm^{-1} and 3250 cm^{-1}.[14] The strong 1580 cm^{-1} peak is due to the *sp2* bonding. The diamond crystal lattice exhibits a sharp peak near 1332 cm^{-1}.[15] The Raman scattering efficiency for the *sp2* 1580 cm^{-1} peak is 55.6 times greater than that for the *sp3* 1332 cm^{-1} peak.[16] A substance with a mixture of *sp2* and *sp3* bonding will have both the 1580 cm^{-1} and the 1332 cm^{-1} peaks. The peaks will also broaden as the degree of disorder increases. Diamond materials are currently characterized by the ratio of the 1332 cm^{-1} peak to the 1580 cm^{-1} peak and by the full width half maximum (FWHM) of the 1332 cm^{-1} peak. Diamond materials may also have non-carbon chemical constituents that also affect their properties. There are six diamond classifications for natural diamond. Each of these divisions is based on different physical properties that are a result of impurities and second phases. Table 1 describes the natural diamond types.

High temperature, high pressure synthetic diamonds are similar to Type 1b natural diamonds.

There are two main types of hard carbon films: diamond-like carbon (DLC) and diamond. Diamond-like carbon films are generally amorphous, but they can also have crystals about 2-20 nm in diameter. DLC contains from ~0-50 mole % hydrogen. DLC films behave like diamond when the carbon gram-atom number densities are above 0.2 $\frac{\text{gram-atoms}}{\text{cm}^3}$. Their film hardness can approach that of diamond films and their amorphous character results in smooth coatings.

Table 1
Natural Diamond Types

Type	Natural Prevalence	Optical Transmission Threshold λ(nm)	Thermal conductivity $\frac{W}{cm°K}$	Resistivity $\frac{\Omega}{cm}$	Impurity	Second Phase
1a	98 %	320	~ 9	> 1.0 x 10^{16}	0.1 % N	None
1b	1 %	320	~ 9	> 1.0 x 10^{16}	<0.05 % N	None
2a	< 1 %	225	~ 26	> 1.0 x 10^{16}	<<0.05 % N	None
2b	<<< 1 %		~ 26	10-1000	B	None
Carbonados	0.2 %	polycrystalline	Variable		Variable	Graphite and others
Ballas	0.2 %	polycrystalline	Variable		Variable	None

Diamond films are defined as single-phase films that are single crystals or with grain sizes greater than 50 nm, if polycrystalline. The film should have a crystalline morphology demonstrating either the four fold symmetry of {100} or {110} surface planes or five-fold symmetry of multiply twinned {111} lattice planes.[17] SEM analysis should reveal cubic, cubo-octahedral, octahedral, pentahedral (evidence of multiply twinned {111} planes), or rounded cauliflower shaped surfaces for polycrystalline films. X-ray or electron diffraction would reveal a single-phase crystalline structure. The Raman spectra must consist of a single, distinct, narrow line at about 1332 cm^{-1}. Low temperature, low pressure synthetic polycrystalline diamond films are similar to carbonados and ballas in their properties. Boron doped ($10^{20} \frac{atoms}{cm^3}$) p-type films have been made with resistivities of $10^{-3} \frac{\Omega}{cm}$. This means that diamond films may be made with resistivities ranging over 19 orders of magnitude. Arsenic doped films show n-type semiconductivity. P-n junctions are therefor possible with diamond. High quality diamond films have excellent optical properties with a high index of refraction and are optically transparent from 225-2000 nm (most excimer, He:Ne, and Ng:YAG lasers) and above 6000 nm (CO_2 lasers).

An exciting new development is the production of high purity ^{12}C diamond films containing about 99.9% ^{12}C.[18,19,20] Normal diamonds have about 1% ^{13}C. The increase in mole fraction of ^{12}C causes a 50% increase in thermal conductivity and about an order of magnitude increase in laser damage tolerance in diamond. Calculations indicate that a 100% ^{12}C defect free single crystal diamond may have a thermal conductivity of about $48 \frac{W}{cm°C}$. Unpublished research indicates that polycrystalline CVD ^{12}C diamond films do not have a higher thermal conductivity than natural isotope abundance CVD diamond films.

4 Mechanism of Vapor Phase Diamond Synthesis

Metastable diamond films may be prepared at much lower temperatures and pressures than equilibrium conditions would require. This is a kinetically controlled phenomena. The exact chemical mechanism of vapor phase diamond deposition is currently unknown.

Many different vapor phase processes can lead to diamond deposition including ion beam deposition, electron beam sputtering of graphite, heated filament techniques, slightly oversaturated (carbon rich) oxyacetylene torches, atmospheric plasma torches, various plasma glow discharge deposition processes including DC,[21] RF,[22] and MW[23] plasmas. Laser enhanced chemical vapor deposition (LECVD) has been attempted by Kitahama *et al.*, but so far it has been unsuccessful.[24,25,26] Many of these techniques use different reactant compounds yet result in microstructurally similar diamond deposits. All of these methods involve vapor phase conditions that result in many reactions becoming significant, leading to very complicated vapor phase compositions. Substrate temperatures for most of these methods must be 800-1000 °C for *sp3* bonded carbon to be the dominant phase. Atomic hydrogen is present in all of these methods. Research on determining vapor phase diamond precursors is very active and the literature results are often contradictory.[27,28,29]

The diamond deposition reaction may be treated in an overall fashion and significant insights may still be made.[30] Consider a generalized deposition reaction of some unknown gas phase hydrocarbon radical that can react to form diamond, graphitizable carbon (true well ordered graphite formation thermal temperatures in excess of 2000 ° C) and atomic hydrogen:

$$C_vH_w \underset{k'_{sp3}}{\overset{k_{sp3}}{\Leftrightarrow}} vC_{sp3} + wH\cdot \qquad [1a]$$

$$C_xH_y \underset{k'_{sp2}}{\overset{k_{sp2}}{\Leftrightarrow}} xC_{sp2} + yH\cdot \qquad [1b]$$

The net rates of deposition, assuming an arbitrary reaction order, are given by:

$$R_{sp3} = \frac{\partial C_{sp3}}{\partial t} = k_{sp3}P_{C_vH_w}^{n_a} - k'_{sp3}P_{H\cdot}^{n_b} \qquad [2a]$$

$$R_{sp2} = \frac{\partial C_{sp2}}{\partial t} = k_{sp2}P_{C_xH_y}^{n_c} - k'_{sp2}P_{H\cdot}^{n_d} \qquad [2b]$$

where the rate constants have the customary Arrenhius temperature dependencies. Gaseous carbon does exist in the thermal equilibrium plasmas and heated filament techniques, and may exist in high electron density non-isothermal plasmas. Consider also the general equilibrium reaction between these unknown hydrocarbon radicals and gaseous carbon immediately above the substrate:

$$C_vH_w \Leftrightarrow v\cdot \dot{\dot{C}}\cdot + wH\cdot \qquad [3a]$$

$$C_xH_y \Leftrightarrow x\cdot \dot{\dot{C}}\cdot + yH\cdot \qquad [3b]$$

having an equilibrium constant:

$$ {}^{C_vH_w}K_{\cdot\dot{C}\cdot} = \frac{P^{v}_{\cdot\dot{C}\cdot} P^{w}_{H\cdot}}{P_{C_vH_w}} \qquad [4a] $$

$$ {}^{C_xH_y}K_{\cdot\dot{C}\cdot} = \frac{P^{x}_{\cdot\dot{C}\cdot} P^{y}_{H\cdot}}{P_{C_xH_y}} \qquad [4b] $$

We can also write chemical equations describing the equilibrium gaseous carbon partial pressures over *sp2* and *sp3* bonded carbon:

$$ C_{sp3} \Leftrightarrow \cdot\dot{C}\cdot \quad ; \quad {}^{C_{sp3}}P^{o}_{\cdot\dot{C}\cdot} \qquad [5a] $$

$$ C_{sp2} \Leftrightarrow \cdot\dot{C}\cdot \quad ; \quad {}^{C_{sp2}}P^{o}_{\cdot\dot{C}\cdot} \qquad [5b] $$

The equilibrium gaseous carbon partial pressure over *sp2* bonded carbon is twice that over *sp3* bonded carbon, according to Badzian *et al.*:[31]

$$ {}^{C_{sp3}}P^{o}_{\cdot\dot{C}\cdot} = 2\,{}^{C_{sp2}}P^{o}_{\cdot\dot{C}\cdot} \qquad [6] $$

Consider a standard gas solution over a polycrystalline solid surface containing both *sp3* and *sp2* bonded carbon regions. Equation [4] is not satisfied because of equation [6]. Draw an analogy of the solid surface to an ideal solution, for purposes of interaction with the vapor phase. Then the degree of supersaturation of gaseous carbon is twice as high over the *sp2* bonded carbon regions than it is over the *sp3* bonded carbon regions:

$$ \frac{P_{\cdot\dot{C}\cdot}}{{}^{C_{sp2}}P^{o}_{\cdot\dot{C}\cdot}} = 2\frac{P_{\cdot\dot{C}\cdot}}{{}^{C_{sp3}}P^{o}_{\cdot\dot{C}\cdot}} \qquad [7] $$

We can consider a pseudo equilibrium state by adding reactions [1] and [5] together, which results in:

$$ C_vH_w \Leftrightarrow v\cdot\dot{C}\cdot + wH\cdot \qquad [8a] $$

$$ C_xH_y \Leftrightarrow x\cdot\dot{C}\cdot + yH\cdot \qquad [8b] $$

We can write a pseudo equilibrium constant for this equation having the form:

$$ {}^{C_vH_w}K^{pseudo}_{\cdot\dot{C}\cdot} = \frac{{}^{C_{sp3}}P^{o}_{\cdot\dot{C}\cdot}\,{}^{v}P^{w}_{H\cdot}}{P^{o}_{C_vH_w}} \qquad [9a] $$

$$ {}^{C_xH_y}K^{pseudo}_{\cdot\dot{C}\cdot} = \frac{{}^{C_{sp2}}P^{o}_{\cdot\dot{C}\cdot}\,{}^{x}P^{y}_{H\cdot}}{P^{o}_{C_xH_y}} \qquad [9b] $$

where $P^{o}_{C_vH_w}$ and $P^{o}_{C_xH_y}$ are determined by setting the rate equation [2] equal to zero and solving:

$$ {}^{sp3}P^{\circ}_{C_vH_w} = \left[\frac{k'_{sp3}}{k_{sp3}} \right]^{\frac{1}{n_a}} P_{H\cdot}^{\frac{n_b}{n_a}} \qquad [10a] $$

$$ {}^{sp2}P^{\circ}_{C_xH_y} = \left[\frac{k'_{sp2}}{k_{sp2}} \right]^{\frac{1}{n_c}} P_{H\cdot}^{\frac{n_d}{n_c}} \qquad [10b] $$

$P_{H\cdot}$ is constant for a given set of operating conditions, making the degree of gaseous carbon supersaturation over *sp3* bonded and *sp2* bonded carbon a function of $P_{C_vH_w}$ and $P^{\circ}_{C_xH_y}$. If we assume that ${}^{i}K_{\cdot\dot{C}\cdot} = {}^{i}K^{pseudo}_{\cdot\dot{C}\cdot}$, then the degree of supersaturation becomes:

$$ \frac{P_{\cdot\dot{C}\cdot}}{{}_{C_{sp^3}}P^{\circ}_{\cdot\dot{C}\cdot}} = \left[\frac{k_{sp^3}}{k'_{sp^3}} \right]^{\frac{1}{vn_a}} P_{H\cdot}^{\frac{-n_b}{vn_a}} P_{C_vH_w}^{\frac{1}{v}} \qquad [11a] $$

$$ \frac{P_{\cdot\dot{C}\cdot}}{{}_{C_{sp^2}}P^{\circ}_{\cdot\dot{C}\cdot}} = \left[\frac{k_{sp^2}}{k'_{sp^2}} \right]^{\frac{1}{xn_c}} P_{H\cdot}^{\frac{-n_d}{xn_c}} P_{C_xH_y}^{\frac{1}{x}} \qquad [11b] $$

Careful analysis of the power coefficients of $P_{H\cdot}$ will lead to the following conclusions. If $n_b/vn_a > n_d/xn_c$, then as $P_{H\cdot}$ increases, the nucleation and growth of *sp2* bonded carbon would be favored over that of *sp3* bonded carbon, which is clearly not the case. Likewise, if $n_b/vn_a = n_d/xn_c$, then for all values of $P_{H\cdot}$ the nucleation and growth of one type of carbon is favored over the other. Therefore, the only case that compares favorably to experimental evidence is $n_b/vn_a < n_d/xn_c$. Considering this latter case, it can be seen from the equation [11] how *sp3* bonded carbon is favored at higher values of $P_{H\cdot}$ and *sp2* bonded carbon is favored at lower values of $P_{H\cdot}$ for constant $P_{\cdot\dot{C}\cdot}$. Therefore, high rate preferential *sp3* bonded carbon deposition requires high gaseous carbon supersaturation over the surface and a high atomic hydrogen partial pressure to inhibit net *sp2* bonded carbon nucleation and growth.

H• has another role as a stabilizer for the *sp3* bonded carbon surface, which contains an unsatisfied *sp3* bond.[32] H• will readily bond to this unsatisfied surface *sp3* bond and prevent the surface layer from collapsing to the more stable *sp2* bonding in the temperature range of 900-1000 °C.[33] Vapor phase halogens will also stabilize the surface unsatisfied *sp3* bond. Therefore, keeping the *sp3* bonded carbon surface from restructuring is an important step that inhibits *sp2* bonded carbon nucleation and growth and allows for further epitaxial growth of *sp3* bonded carbon.

The presence of oxygen in the vapor phase has been shown experimentally to greatly increase the preferential deposition of *sp3* bonded carbon. The above analysis does not consider the role of oxygen on the degree of supersaturation of gaseous carbon over *sp3* bonded and *sp2* bonded carbon. However, it is well known that *sp3* bonded carbon is much more oxidation resistant than *sp2* bonded carbon.[34] Perhaps the role of oxygen is to increase the etch rate of *sp2* bonded carbon. Expanding the above analysis to include the effect of an oxygen containing vapor phase, consider the reaction of atomic oxygen to remove solid carbon:

$$C_{sp3} + p\dot{O} \underset{k_{O_{sp3}}}{\overset{k'_{O_{sp3}}}{\Leftrightarrow}} CO_p \qquad [12a]$$

$$C_{sp2} + s\dot{O} \underset{k_{O_{sp2}}}{\overset{k'_{O_{sp2}}}{\Leftrightarrow}} CO_s \qquad [12b]$$

If we assume that $k'_{O_{sp3}} \gg k_{O_{sp3}}$ and $k'_{O_{sp2}} \gg k_{O_{sp2}}$ then the net rates of deposition becomes:

$$R_{sp3} = \frac{\partial C_{sp3}}{\partial t} = k_{sp3} P_{C_vH_w}^{n_a} - k'_{sp3} P_{H\cdot}^{n_b} - k'_{O_{sp3}} P_{\dot{O}}^{n_e} \qquad [13a]$$

$$R_{sp2} = \frac{\partial C_{sp2}}{\partial t} = k_{sp2} P_{C_xH_y}^{n_c} - k'_{sp2} P_{H\cdot}^{n_d} - k'_{O_{sp2}} P_{\dot{O}}^{n_h} \qquad [13b]$$

Perceiving that $k'_{O_{sp2}} > k'_{O_{sp3}}$, one can see from equation [13] that the presence of oxygen in the diamond depositing atmosphere will allow the partial pressure of the hydrocarbon to be increased for the same deposit quality.

5 Transport Phenomena In LCVD and LECVD Systems

The phenomena of momentum, heat, and mass transport are critically important in the proper design of a real LCVD or LECVD system and in understanding the resulting deposit phase, microstructure, and material properties. High rate deposition may be a transport limited process. The gas phase reactants and reaction products must flow through the reactor. The laser beam heats a small region of the substrate or previous deposit at any instant in time. This heat is dissipated through heat conduction, convection, and radiation. The reactants and reaction products must be transported to and from the reaction zone through the combined effects of diffusion and momentum transport. In general, the resulting partial differential equations for diffusion, momentum, continuity, and heat conduction are coupled together and therefore must be solved simultaneously. The standard assumption of negligible convective and radiative heat transfer may be then tested by comparing the resulting conduction heat flux with the heat flux from convective heat transfer correlations and black body radiation.

5.1 Photon Heating

Proper control of laser induced substrate heating is critical for solid freeform fabrication of diamond. The thermal processing window for diamond deposition is between 800-1100 °C. Light energy can result in thermal heating of a media through absorption. The general equation for heat flow by conduction into semi-infinite slabs neglecting heat losses due to conduction, convection, and radiation to the surrounding medium is given by:

$$\rho_i(T) C_p(T) \frac{\partial T}{\partial t} - \nabla[K(T)\nabla T] = Q(t) \qquad [14]$$

$$Q(t) = I_o A(T, \lambda, \Theta) \qquad [15]$$

where $Q(T)$ is the heat source from a laser beam incident on the surface. Consider the case of a laser beam incident on a gas-solid interface oriented perpendicular to the beam. At time zero the beam is turned on. Herziger[35] solved the transient heat conduction equation for the center

of the beam assuming a Gaussian beam intensity distribution, temperature independent material properties, and no phase transition latent heat effects:

$$T(0,0,0,t) = \frac{AI_o r_f}{2K\sqrt{\frac{\pi}{2}}} \arctan\sqrt{\frac{8\alpha t}{r_f}} \qquad [16]$$

The assumptions of constant material properties and zero latent heat made to develop the closed form solution severely limit its applicability to real-world situations because C_p and K can change over an order of magnitude over a 1000 °C temperature range. Accurate modeling of photon heating requires open form, iterative numeric solutions.[36]

5.1.1 Substrate and Deposit Vapor Pressure

The local substrate or deposit vapor pressure is only a function of the local temperature of the material. Relations between vapor pressure versus temperature have an empirical nature. Such vapor pressure relations often have of form:

$$\ln P^{sat} = A - \frac{B}{T+C} + DT + E\ln T \qquad [17]$$

where A, B, C, D, and E are constants. When D = E = 0, equation [15] is called the Antoine equation. When the vapor pressure of the material within the heated zone equals or exceeds the system pressure, rapid local vaporization of material proceeds. Figure 1 shows experimental gaseous carbon vapor pressure[37] and a least squares fit to equation [15] assuming that C=500.

The substrate or deposit vapor itself has an absorption coefficient that can be non-trivial. Therefore, vaporization of material can and usually does increase the coupling of laser energy into the substrate or deposit by absorbing both incident and reflected laser energy. This energy is transferred to the substrate through both heat conduction and radiation heat transfer mechanisms as well as by vapor condensation with consequent release of latent heat.

This process is quite unstable in nature and acts like a positive feedback control system. Usually the reflection of a material decreases markedly upon a solid to liquid phase transition. This usually leads to a corresponding step increase in photon absorption, which in turn leads to a step increase in the temperature rise per unit time. When the vapor pressure equals the system pressure, another step increase in energy coupling to the substrate occurs. This causes the substrate or deposit temperature to rise even faster, greatly increasing the local pressure near the incidence of the laser beam to the substrate. Soon the vapor temperature and pressure are high enough to create a plasma.

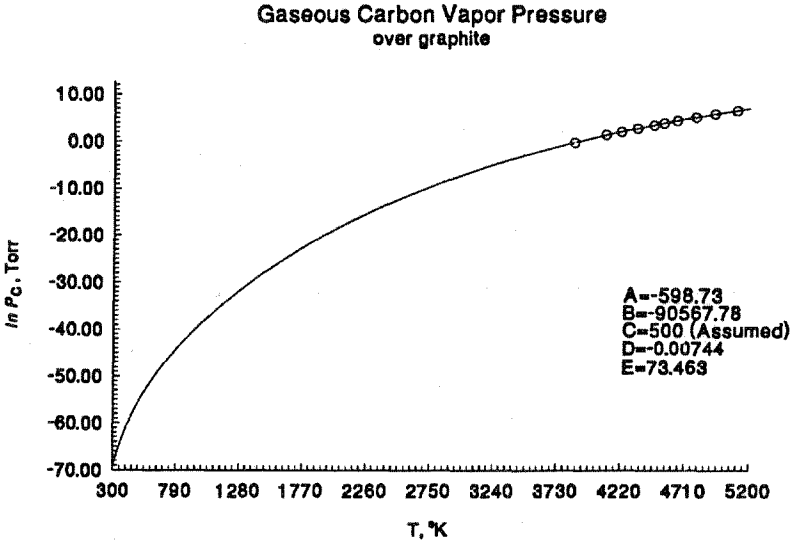

Figure 1: Gaseous carbon vapor pressure over graphite versus temperature.

5.2 LCVD Reaction Rate Limiting Regimes

An extremely important issue in LCVD and LECVD is the total rate of deposition. Analysis of this parameter is totally dependent upon the variables of a specific system.

The process of chemical reaction and deposition is complicated and multistep by nature. Bauerle[38] has identified seven consecutive steps in laser-induced reactions:

1. Transport of reactants into the reaction zone through the boundary layer.
2. Adsorption of one or more reactants onto the substrate.
3. Pyrolytic or photolytic activation of molecules near or at the substrate surface.
4. Transport of product atoms or molecules to the substrate surface, with possible recombination or secondary reactions on the way.
5. Condensation or further reactions of the products of step 3 on the surface.
6. Desorption of reaction products from the substrate.
7. Transport of reaction products out of the reaction zone and through the boundary layer.

Each of these steps proceeds at a certain rate. The total process can proceed no faster than the slowest step, the rate limiting step.

At low surface temperatures for LCVD or low laser intensities for LECVD the rate of deposition is usually limited by reaction kinetics. Past a critical temperature, the reaction rate becomes diffusion limited. Reactants or reaction products can not diffuse through the boundary layer faster than the reaction proceeds. The reaction rate in this regime is a function of the thickness of the boundary layer, the bulk concentration of the reactants and products, the temperature and the pressure, and the laser pulse time.

5.2.1 Momentum Boundary Layers in LCVD and LECVD

A boundary layer develops whenever a fluid flows over a surface with a different relative velocity. A boundary layer is a regime with a different velocity than the bulk fluid. The thickness of a boundary layer is defined as being that distance from the surface where the velocity of the fluid reaches 99 % of the free-stream velocity. The value of the local Reynolds number determines the type of the boundary layer:

$$\mathrm{Re}_x \equiv \frac{x v \rho}{\mu} \qquad [18]$$

where x is defined as the distance from the leading edge of the plate. For the case of flow over a flat plate the following flow regimes are experimentally found:

$Re_x < 2 \times 10^5$ the boundary layer is laminar

$2 \times 10^5 < Re_x < 3 \times 10^6$ the boundary layer is in transition

$3 \times 10^6 > Re_x$ the boundary layer is turbulent

However, for most real reactor designs, such simplistic analysis techniques have no relevance.

Consider an area large relative to the incident laser beam diameter where it is desired to have an even reaction rate so that scan velocities may be constant over the whole area for all scan times. It is desired then to have an even, non-turbulent boundary layer in order to control the reaction rate if the deposition is in the desired diffusion limited regime necessary for high rate deposition. The best way to determine if such a boundary layer exists is to perform a finite element analysis of the flow field.

5.2.2 Diffusion Boundary Layers In LCVD And LECVD

The reaction reactants and products get to and from the reaction site by both momentum and diffusive transport. When the reaction kinetic rate is sufficiently high, the development of a diffusive boundary layer will result.

To understand the fundamentals of mass transfer, it is beneficial to review some basic equations. Fick's first "law" of diffusion is, relative to the molar average velocity v:

$$\mathbf{J}_A^* = -c\,\mathrm{D}_{AB} \nabla x_A \qquad [19]$$

For an ideal gas, equation [19] may be rewritten:

$$\mathbf{J}_A^* = -\frac{P}{RT}\mathrm{D}_{AB} \nabla x_A \qquad [20]$$

For a mixture of gases, the diffusion coefficient may be estimated from the Fuller correlation:

$$\mathrm{D}_{AB} = \frac{10^{-7} T^{1.75} \left(\frac{1}{\mathrm{M}_A} + \frac{1}{\mathrm{M}_B} \right)^{1/2}}{P[(\Sigma \upsilon)_A^{1/3} + (\Sigma \upsilon)_B^{1/3}]^2} \qquad [21]$$

Note in particular that the molar flux is a function of the temperature raised to the three quarter power. Fick's second "law" of diffusion is:

$$\frac{\partial c_A}{\partial t} = \mathrm{D}_{AB} \nabla^2 c_A \qquad [22]$$

The characteristic diffusion time mentioned above is defined as the time required to reduce the concentration gradient to 1 % of its greatest value. The characteristic diffusion time is found by solving equation [22] for a particular set of initial and boundary conditions.

The type of diffusion boundary layer in CVD systems is highly dependent upon the nature of the deposition. Figure 2 illustrates the two major types of diffusion boundary layers that are found in CVD of planer substrate surfaces. Figure 2a and 2b show the development of a hemispherical boundary layer that develops when the laser beam scan velocity is slow relative to the characteristic diffusion time, but the time between scan lines is either slow or fast. This results in three dimensional diffusion. Figure 2c and 2d show the development of a planer diffusion boundary layer. A planer boundary layer will occur when the scan lines are either contacting for LECVD or overlapping for LCVD and the time for a complete scan over the total deposition area is short compared to the characteristic diffusion time needed to replenish the depleted zone. This results in one dimensional diffusion identical to large area CVD.

The effect of the type of diffusion boundary layer on the deposition rate is profound. Allen *et al.*[39] claim that for favorable reactant systems, very rapid deposition rates (greater than $100\frac{\mu m}{sec}$) and scan speeds for line deposition (greater than $10\frac{cm}{sec}$) can be achieved. However, such deposition rates are found only for the case of a hemispherical diffusion boundary layer that one would not find occurring in large area rapidly scanned material processing using laser beams.

Bauerle[40] modeled a simple case assuming negligible surface diffusion and convective flow. He also assumed that the reactant diffusion is much slower than product diffusion. The time dependent surface reaction flux (proportional to deposition rate) for a hemispherical diffusion boundary layer is given by:

$$j(t)=\frac{2\mathrm{D}\,C_\infty}{l_o+d}\left\{1+\frac{d}{l_o}e^{\left(\frac{1}{l_o}+\frac{1}{d}\right)^2 4\mathrm{D}t}\,erfc\left[\left(\frac{1}{l_o}+d_o\right)(4\mathrm{D}t)^{\frac{1}{2}}\right]\right\} \qquad [23]$$

where at time zero the reaction begins. l_o is a length scale proportional to the mean free path in the gas and is defined as:

$$l_o=\frac{4\mathrm{D}}{\eta' v_m} \qquad [24]$$

The time required to reach steady state is:

$$\tau_o \approx \frac{l_o^2 d^2}{4\mathrm{D}\,(d+l_o)^2} \qquad [25]$$

Because $\mathrm{D}\propto P^{-1}$,

$$\tau\propto P \qquad \text{for} \quad d \ll l_o$$

$$\tau\propto P^{-1} \qquad \text{for} \quad d \gg l_o$$

τ can be < 10 ns for small spot sizes and pressures below one atmosphere, such as what occurs in microchemical processing. For steady state deposition, apply L'Hopital's Rule:

$$j(t\rightarrow\infty)=\frac{2\mathrm{D}\,C_\infty}{l_o+d} \qquad [26]$$

which again yields two limiting cases:

$$j(t\rightarrow\infty)\propto P \qquad \text{for} \quad d \ll l_o$$

$$j(t\rightarrow\infty)\propto\frac{1}{d} \qquad \text{for} \quad d \gg l_o$$

Copley studied mass transport during LCVD and concluded that reaction rates can be characterized into three regimes depending upon the molar ratio of vapor phase reactants to products, bulk mole fractions, and kinetic rates.[41] The slowest rates are kinetically controlled, where no mass transport limits are found for either reaction products or reactants. The second case is where the molar ratio is one or more, where more moles of reactants are diffusing to the surface than moles of products are diffusing away. The molar average velocity is towards the substrate. This is a diffusion limited regime, and some limitation is placed upon the kinetic rates. The third regime Copley studied is the case when the molar ratio is less than unity, where the outward diffusion of products impedes the inward diffusion of reactants. He calls this case the diffusion plus convective case and the molar average velocity is away from the substrate. This regime provides the most impediment to the kinetic rate.

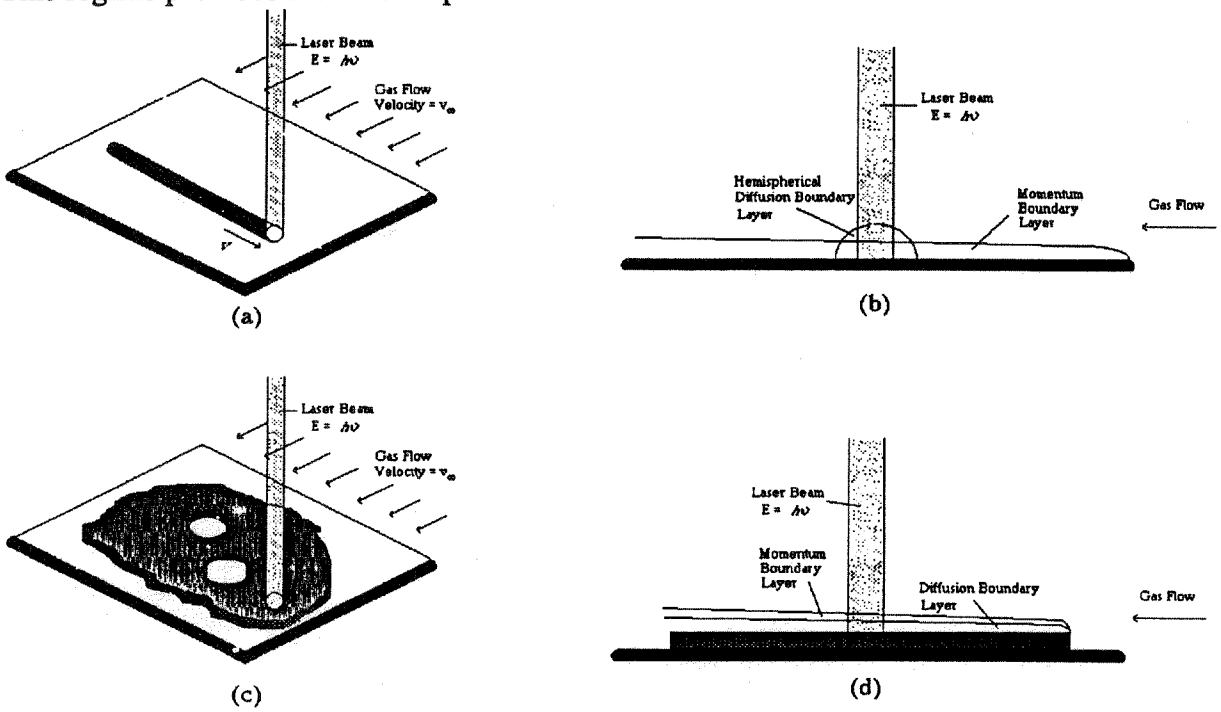

Figure 2: Two limiting conditions of diffusion boundary layers in LCVD and LECVD systems: (a) & (b) show vertical and horizontal views of a hemispherical diffusion boundary layer occurring when the scan velocity v << characteristic diffusion time; (c) & (d) show vertical and horizontal views of a planar diffusion boundary layer that develops when the time for a complete scan >> characteristic diffusion time and the scan lines contact or overlap.

5.3 Spatial Confinement In LCVD and LECVD Systems

It is important to confine the deposition of product to the area immediately adjacent to the laser beam in order to produce parts with a high degree of definition. This is in direct conflict with the desire to minimize the boundary layer thickness in order to increase the deposition rate for LECVD. The most common method for increasing deposition rate at constant P is to increase flow velocity over the substrate, thereby minimizing the momentum and diffusion boundary layer thickness. For LCVD systems where the reaction mechanism occurs by surface decomposition of reactant, this poses little conflict. However, in LECVD reaction mechanisms, analogies may be drawn to plasma enhanced chemical vapor deposition (PECVD), where

deposition often occurs by the creation of activated species, usually free radicals or diradicals, in the gas phase and diffusion of these short lived species to the surface where the deposition reaction occurs.[42,43,44,45]

In LCVD reaction schemes for large area deposition, the spatial confinement is defined by the reaction kinetic and heat transport equations. For single line deposition, the deposit will always have a diameter smaller than the beam diameter for endothermic reactions, because the incident beam diameter intensity follows a Gaussian dependence on radius and the reaction kinetics have an exponential dependence on temperature. For large area deposition, bulk versus surface heating effects must be investigated. For example, consider the hole in Figure 2c. Assume the dark region around the hole is hotter than the white hole, thereby allowing for CVD to occur. In order to maintain constant boundary definition with increasing deposit thickness, it is important to insure that the cold area (hole) can transfer heat from its surface as fast as the hot area (dark region) transfers heat into it. This may be accomplished by transferring heat from the substrate, using a low temperature gas feed, and by decreasing the absorption length to increase the temperature gradient at the surface and minimize bulk heating effects.

In LECVD reaction schemes, the creation of energetic species occurs throughout the incident laser beam diameter. Deposition occurs more evenly throughout the beam incidence and even a little beyond the beam due to diffusion effects. In a flow field, deposition can occur downstream of the beam.

One measure of the reaction spatial confinement of a plasma is the mean free path of the molecular species. The mean free path of an ideal gas is given by:

$$\Lambda = \frac{\kappa T}{\sqrt{2}\,\pi\sigma^2 P} \qquad [26]$$

At 1000 °K and 1 atm. pressure, $\Lambda = 2.34x10^{-7}$ meters for air. The mean free path specifies the average distance gas phase molecules travel between collisions with other gas phase species. One often assumes that a collision of a radical with another gas phase molecule always results in a reaction. This distance is sufficiently small to ensure adequate spatial confinement. However, if the system pressure is 10^{-6} atmospheres, this criterion is no longer sufficient. One must resort to more complicated estimates of excited state mean relaxation times of excited species.

6 Design Of The Remote Plasma Solid Freeform Fabrication Vapor Phase Reactor System

6.1 Design Requirements

High rate nucleation and growth of diamond requires a high local partial pressure of atomic hydrogen. Localized, controlled deposition of diamond requires localized substrate heating apparently within the thermal processing window of 800-1100 °C. The reaction chamber is designed to adapt on the existing REMPITOFMS system. The system must have mass flow controllers for all of the process gases as well as chamber pressure control. The substrate heater must heat to 1100 ° C so that large area deposits may be grown without use of the laser. The heater must have a temperature controller. The reactor wall must be water cooled to prevent overheating from the substrate heater. The reactor must be designed to that it is convertible so that a plasma may be created in the chamber over the substrate by TM_{01} mode. Parallel gas flow over the substrate surface will lead to thinner boundary layers.

6.2 Plasma System

Atomic hydrogen will be created by a plasma system. A microwave plasma source was chosen over RF due to the greater power coupling available at the shorter wavelength of the microwaves. A downstream microwave plasma system is used, operating at 2.45 GHz and available from ASTEX, Inc. This system is schematically shown in Figure 3. It is capable of supplying up to 1.5 kW of microwave energy. The design of the downstream microwave plasma reactor tube must allow the metastable (neutrals) excited species created in the plasma to be transported to the substrate for low pressure operation in the 10^{-2} Torr range. Therefore the tube wall must be an electrical insulator and withstand temperatures above 1000 °C in the microwave coupler. The inner tube wall surface is electrically insulating downstream of the plasma coupler to prevent charged specie recombination. A conventional alumina tube (McDanel Type 998) of 1.5" O.D. is used to transport the metastable species to the reaction chamber. For operation at pressures above 100 Torr, a 1/4" O.D. alumina tube is used as the reactant supply line in the center of the 1.5" O.D. tube to increase energy density of the excited stream. The plasma system is designed so that substrates may be placed in and downstream of the plasma so that the effects of downstream recombination on deposit characteristics and growth rate may be studied. The alumina tube may be cooled by a water jacket or heated by a resistance wire wrap as desired.

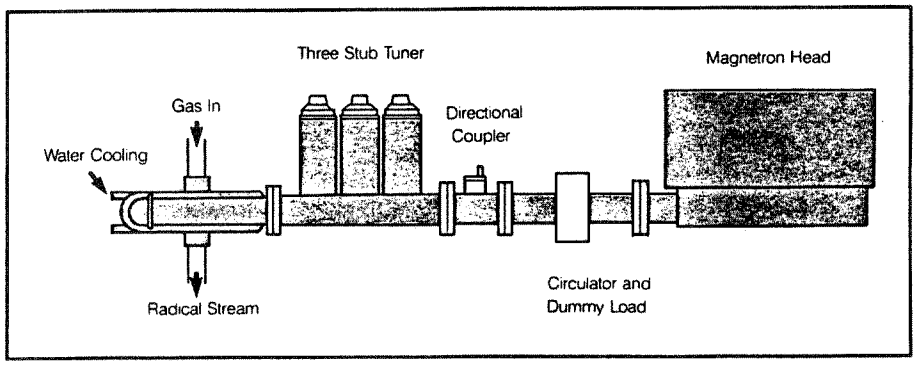

Figure 3: The 1.5 KW downstream microwave plasma system.

6.3 Reaction Chamber

The reactor chamber is shown in Figure 4 and 5. Table 2 describes the labels in Figure 4. The reactor is water cooled by a double wall jacket. The top lid of the reactor is convertible to allow for a symmetric TM_{01} mode plasma coupler to fit on it over a 5" ZnSe CO_2 laser window. In this mode the laser scanning mirrors are placed in the cylindrical coupler. This will allow for a plasma to be created directly over the substrate in the future. Currently, it has a 2" ZnSe CO_2 laser window at the top. The laser optics and scanning system are above the reactor. It has 4 ports mounted at 30° from the substrate to allow for video imaging and *in situ* laser interferometry of the growing deposit. A capacitive manometer is placed on one of these ports. The reactor has a fast entry port. The bottom lid of the reactor is an ISO-250 flange that is removable for reactor mounting on the REMPITOFMS system. The substrate heater and hydrocarbon feed line are mounted on the bottom lid. K-type thermocouple feedthroughs are mounted on a port opposite of the door port. The reactor is designed so that the process gases flow parallel to the substrate and the laser beam impinges perpendicular to the substrate.

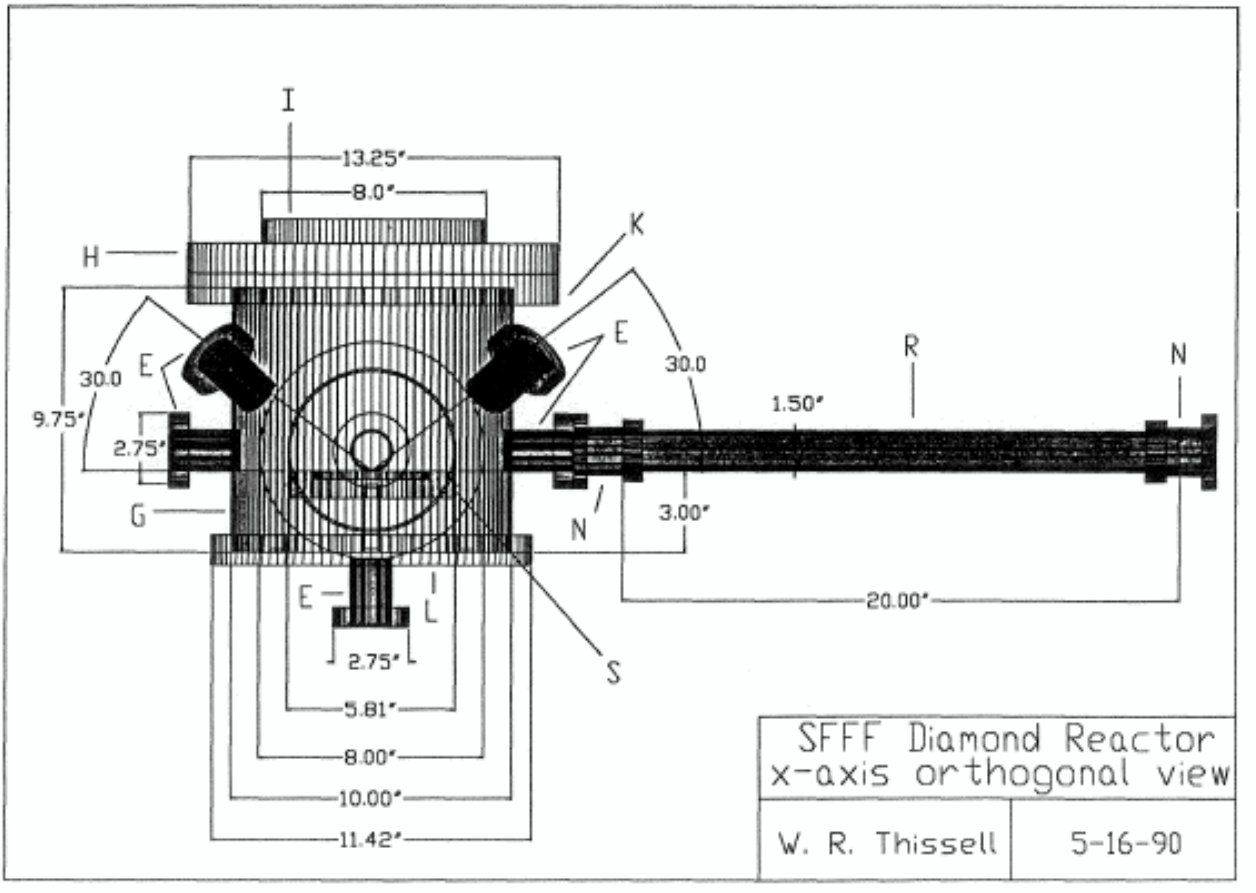

Figure 4: X axis orthogonal view of the SFF diamond reactor.

Table 2
Part Descriptions for Figure 4

Figure 4 label	Description
E	Conflat port
G	Double wall water cooled reactor wall
H	Conflat reducing flange
I	8" to 3-3/8" Conflat reducing flange with 2" laser window
K	Conflat flange
L	ISO-250 flange
N	Conflat to 1-1/2" tube Vac-Coupling
R	Al_2O_3 tube
S	1100 °C substrate heater

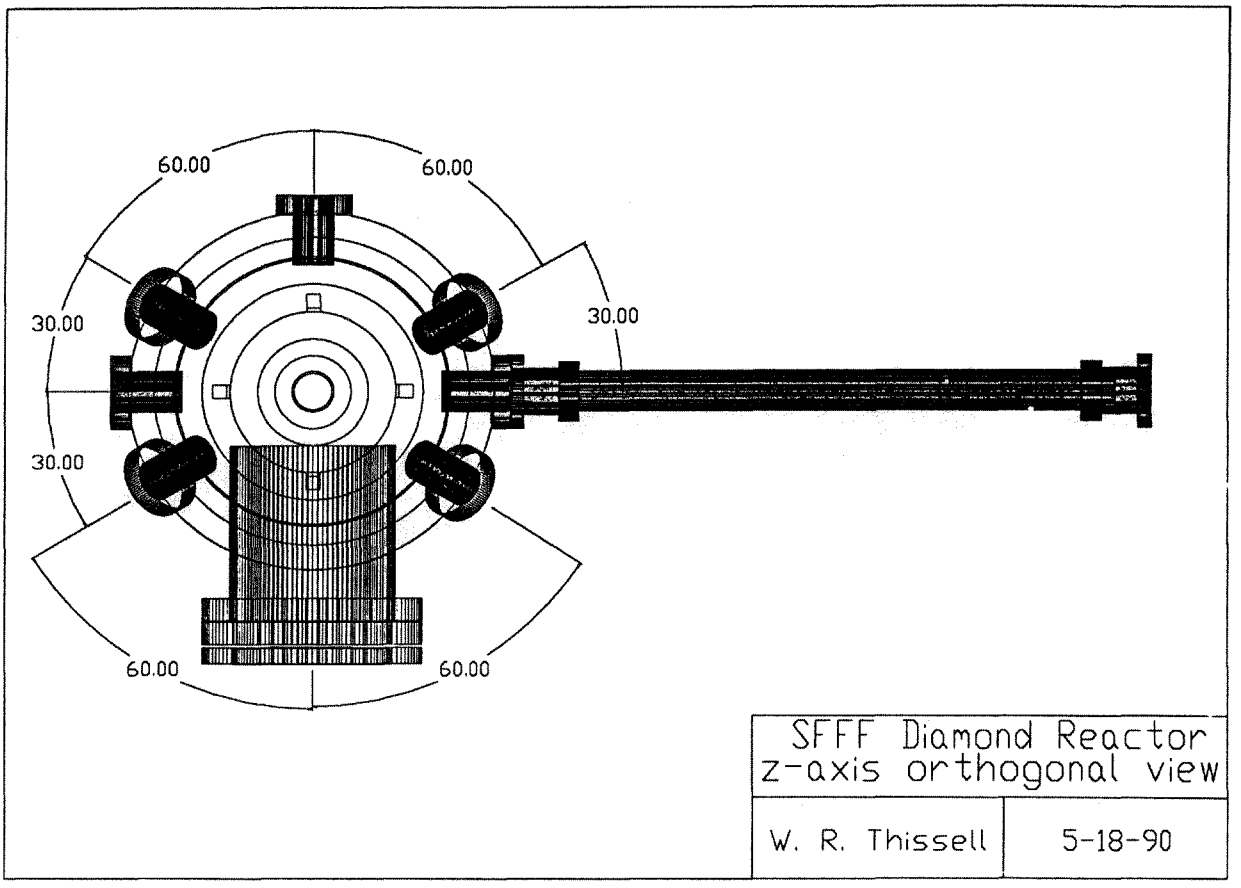

Figure 5: Z axis orthogonal view of the SFF diamond reactor.

6.4 Substrate

The requirements for the substrate is that it must be flat, smooth, capable of withstanding temperatures above 1000 °C, and be stable in an hydrogen and oxygen plasma. Many materials have these characteristics such as Si and Al_2O^3. The substrates will be prepared before each run by a diamond paste polish to below 1 μm grit size followed by an ultrasonic rinse for 5 minutes in each of four solvents: glacial acetic acid, reagent grade I water, methanol, and acetone. Before each part is made, an even primary layer of amorphous carbon with a thickness of 25 μm is deposited over the entire substrate by sputtering or PECVD. This carbon layer's purpose is to facilitate even nucleation of diamond over the entire substrate wherever the laser is incident. Silicon is transparent to 10.6 μm photons below 700 °C, while amorphous, *sp2* bonded carbon is opaque to this photon energy. Although low defect density diamond films are transparent to 10.6 μm photon energy, the high rate deposition planned for SFF will result in high defect density *sp3* bonded deposits that will be opaque. Deposition rates may be lowered for growth of high quality *sp3* bonded films that will have good optical transparency characteristics.

6.5 Substrate Holder and 1100 °C Heater

The choice of materials and heater design was motivated to achieve several design goals. The heater must be inexpensive. RF induction heating of a graphite substrate was eliminated because of its cost and large heated volume. Halogen lamps were similarly eliminated due their cost and nonuniform heating. A conventional ohmicly heated resistance wire heater was chosen

for economy. The wire is embedded in a ceramic plate mounted on a ceramic support. The hydrocarbon feed is directly upstream of the substrate and is designed to evenly distribute the hydrocarbons over the leading width of the substrate heater. The substrate (silicon wafer) will rest on the heater. A great concern is the projected lifetime of the Cr-Al-Fe alloy heating element in a hydrogen and oxygen atmosphere. Hydrogen embrittlement, oxidation, and sulphur induced green rot can both cause heater element failure, but the projected lifetime is hard to estimate. The heater support and chamber are designed to facilitate heater replacement.

7 Computational Plasma Modeling

Multi-element containing plasmas are inherently complex systems because of the large number of non-trivial chemical reactions that can occur within them. Reproducible and predictable high rate diamond deposition requires a fundamental understanding of the concentrations of the suspected diamond vapor phase precursor chemical species within the plasma and downstream of the plasma. Understanding the kinetic balance between net *sp3* bonded carbon deposition and net *sp2* bonded carbon deposition also requires an understanding of the concentrations of the relevant vapor phase chemical species.

Plasma modeling and plasma diagnostics are necessary to reach this level of understanding, and are absolutely required before significant process scale up may be reliably achieved. Carbon and hydrogen containing plasmas have been well modeled in the literature. Kline *et al.* modeled a methane RF glow discharge plasma using a Monti-Carlo simulation of electron molecular species interactions.[46] The authors concluded that $CH_3\bullet$ were the primary carbon deposition species. He also used the plug flow model to predict specie concentrations downstream of the glow discharge. This assumption is good for species with characteristic time constants below 1 milliseconds, which included most species. The reactive species that exit the glow discharge zone were found to rapidly decay to equilibrium species. Tachibana *et al.* performed plasma diagnostics and modeled a methane plasma used to deposit amorphous carbon.[47] Their model included 15 neutral chemical species, 20 ionic chemical species and 23 neutral chemical reactions and 33 ionic reactions. Their model predicted that the most abundant neutral radical in the plasma is $CH_3\bullet$. They found that the rate of change in the partial pressure of CH_4 with respect to time is nearly proportional to the RF forward power of the plasma:

$$\gamma_{CH_4} = -\frac{\frac{\Delta P_{CH_4}}{\Delta t}}{P_{CH_4}} \qquad [27]$$

They also found that the ratio of γ_{CH_4} over the RF power in W decreases as the pressure increases. Suzuki *et al.* modeled a DC discharge plasma under diamond deposition conditions.[48] They diagnosed their plasma using the Langmuir probe technique and optical emission spectroscopy. They modeled their plasma assuming that the neutral species are in a thermal equilibrium state because the degree of ionization is low ($\sim 10^{-7}$) and the total gas pressure is about 200 Torr. They found that almost all of the CH_4 is decomposed to $\cdot\dot{C}\cdot$ and H• at the statistical temperature above 4,800 K where diamond was observed to grow. They concluded from this result that the formation of $\cdot\dot{C}\cdot$ plays a significant role for diamond growth.

The importance of good complete reaction rate data in plasma modeling cannot be overemphasized. The highest growth rates of diamond deposition from the gas phase are reported to be from oxygen containing vapor phases, but it is not known why. Therefore, oxygen containing plasmas are worth of study. Oxygen, carbon, and hydrogen containing plasmas will be modeled using the CHEMKIN II software package available from Sandia National

Laboratories. The plasma model results will be crucial to understanding why higher diamond deposition rates are reported in the literature for oxygen containing plasmas and at higher feed ratios of CH_4/H_2.

8 Plasma Diagnostics

Plasma electron energies and densities are important input parameters for the computational plasma species model. Both of these parameters will be obtained by use of the Langmuir probe technique.

Many techniques are available to perform transient specie analysis in the plasma. Such techniques include: optical emission spectroscopy (OES)[49], coherent anti-Stokes Raman spectroscopy (CARS),[50,51] resonance enhanced multiphoton ionization (REMPI),[52,53,54,55,56,57] and resonance enhanced multiphoton ionization time of flight mass spectroscopy (REMPITOFMS). OES provides a line of sight averaging of information through the plasma. CARS is not sufficiently developed at this time to be a useful technique. REMPI provides very good line of sight averaging of information like OES, but resonant frequency overlap among several different species can lead to misinterpretation of experimental data. REMPITOFMS promises to provide good concentration data of the vapor phase transient species immediately above the depositing film down to 10^{-8} mole fraction. By combining time of flight mass spectroscopy (TOFMS) with REMPI, REMPITOFMS will allow the relative contributions to be made of all species having overlapping resonant ionization frequencies. REMPITOFMS will be used to qualitatively determine transient specie concentrations within and downstream of the plasma. The REMPITOFMS results will be compared to the computer model results.

A 2+1 REMPI process is shown schematically in Figure 6. Two photons of the same energy excite an electron in the molecule to an excited state. Another photon of the same energy is sufficient to eject the electron from the molecule. The excited state is short lived and the molecule may also fluoresce, releasing a photon and dropping down to a lower energy level. The exited state may also decay by intramolecular relaxation. Not all REMPI processes are 2+1; 3+1 and 4+1 ionizations are also found.

Figure 7 shows schematically the REMPITOFMS diagnostic station. The remote plasma diamond SFF reactor is placed on top of the REMPITOFMS system, replacing the substrate heater and bottom ISO-250 flange of the reactor with the diagnostic station substrate heater and ISO-250 flange. A molecular beam is introduced into the REMPI column through a hole of 50-250 μm in diameter etched in a silicon wafer. The sampling volume of the reactor is a hemisphere of diameter 3-5 times the hole diameter. The sampling funnel is designed so that once molecules enter the REMPI column they do not undergo any collisions. The pressure in the SFF diamond reactor is maintained at 0.01-730 Torr by a mechanical pump and proportional flow control valve; while the REMPI column is maintained at about 5×10^{-8} Torr by two turbomolecular pumps.

Specific species are ionized by the tunable dye laser by the REMPI process. Once ionized, they are accelerated and focused by electrostatic lenses to a Chevron plate detector in a conventional time of flight mass spectrometer. The TOFMS gives all the ions produced by a single laser pulse the same momentum. The velocity of the ions in collision-free flight is a function of the ratio of their charge, q, to their mass, m. TOFMS is well described in the literature.[58]

REMPITOFMS will answer many questions on the nature of *sp3* bonded carbon deposition. The substrate temperature may effect the concentration of the gas phase species above it. The effect of the distance from the plasma to the substrate on gas phase specie concentrations at various pressures may also be studied. The effect of plasma power, the mole fraction of input

gases, and total flow rates on gas phase specie concentrations may also be studied. Relating the REMPITOFMS results to deposit characteristics and computational models will answer many questions.

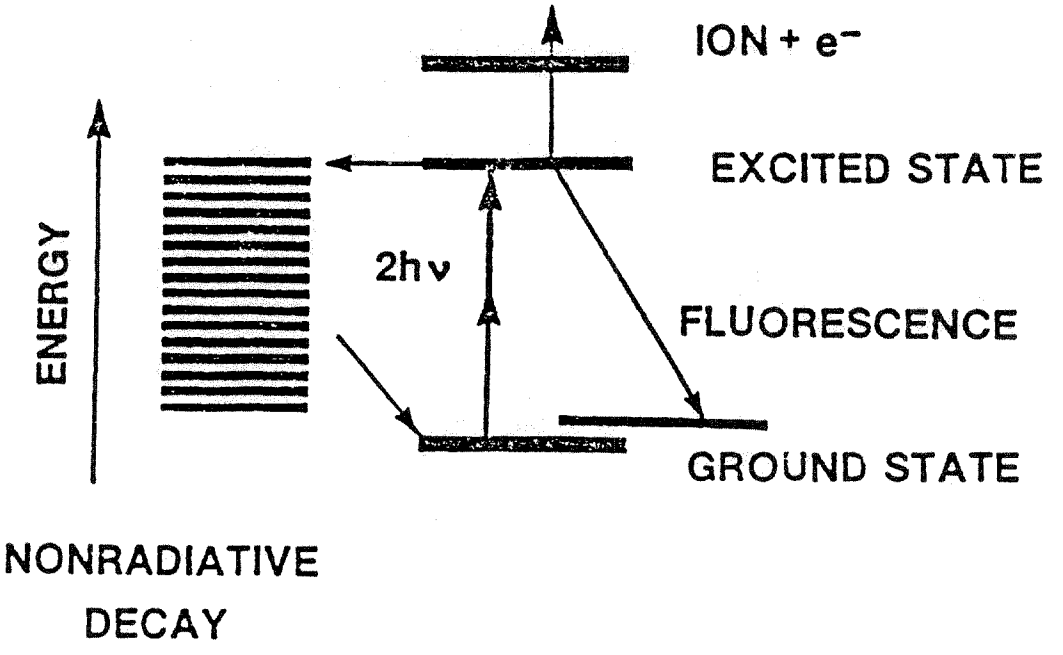

Figure 6: Schematic drawing of a 2+1 REMPI process. Two competing processes for the excited state are intramolecular relaxation (nonradiative decay) and fluorescence.[59]

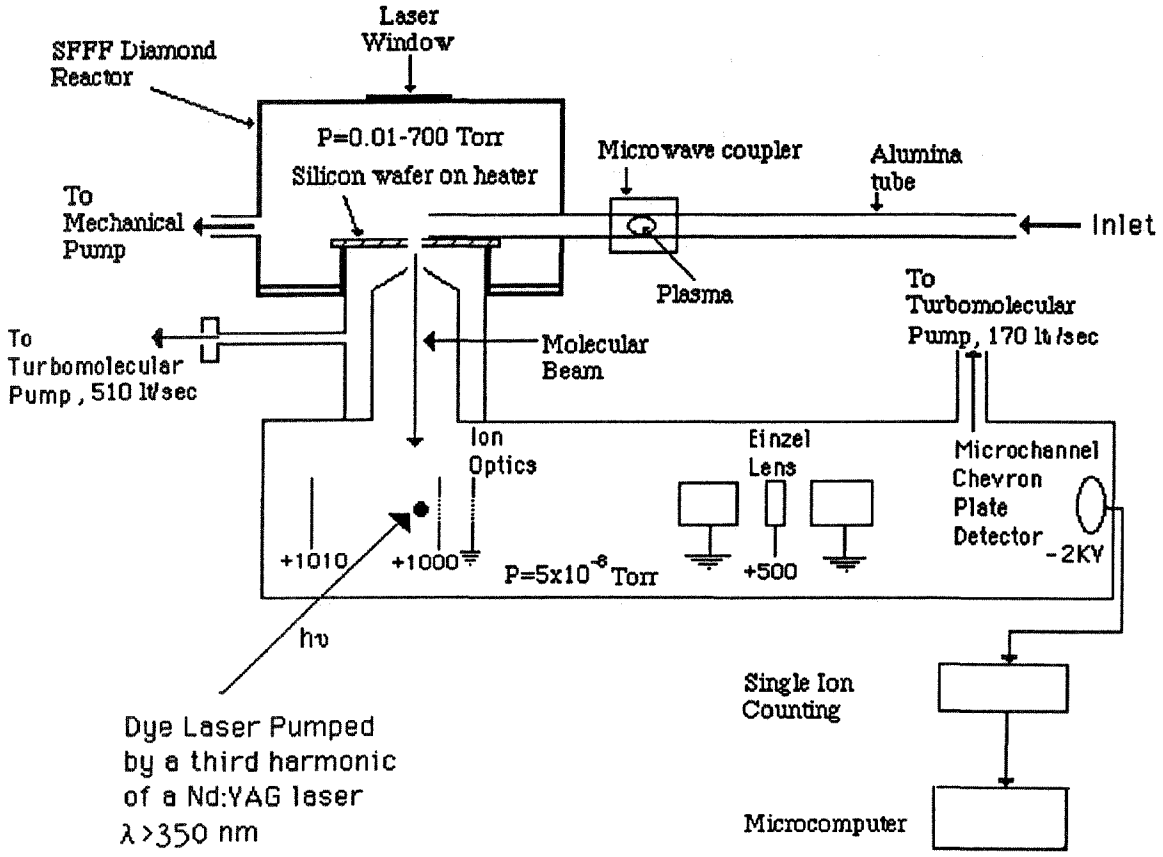

Figure 7: Schematic drawing of the REMPITOFMS diagnostic station. The SFF diamond reactor is shown on top of the station.

9 Summary

Metastable *sp3* bonded carbon deposition growth rates have increased from the Å/hr range for hot wire techniques in the early 1980's to 930 μm/hr for thermal equilibrium argon-hydrogen plasma torches with downstream methane injection in 1989.[60]

Thermodynamic, kinetic, and transport phenomena theories suggesting that even higher growth rates are possible have been discussed. The design of a vapor phase solid freeform fabrication reactor for fabricating *sp3* bonded carbon parts has been described. The reactor is designed to allow for high rate deposition of *sp3* bonded carbon by both remote plasma LCVD and *in situ* plasma enhanced LCVD.

The problems preventing high rate deposition of *sp3* bonded carbon will be attacked through the triad of experimentation, modeling, and diagnostics. The knowledge gained from these studies will be incorporated into next generation reactors resulting in faster production, greater spatial definition, and more structurally sound solid freeform fabrication parts.

10 Acknowledgements

The authors would like to acknowledge Steve Lin and Norman Williams for numerous discussions on gas handling and vacuum system design and implementation. The authors greatly appreciated the assistance of Justine Hager and Professor Eckerdt of the Chemical Engineering Department for guidance in designing REMPITOFMS compatability into the system design. This project is sponsored by the Texas Advanced Technology Program.

References

1. Bachman, P. and R. Messier, "Emerging Technology of Diamond Thin Films," Chemistry and Engineering News, May 15 1989 24-39.

2. Evans, T., "Changes Produced by High Temperature Treatment of Diamond," in Properties of Diamond, edited by J. E. Field, New York: Academic Press, 1979, 403-24.

3. Angus, J., "History of Diamond Growth at Metastable Conditions," Proceedings of the First International Symposium on Diamond and Diamond-like Films, edited by Dismukes, J. P., A. J. Purdes, B. S. Meyerson, T. D. Moustakas, D. E. Spear, F. V. Ravi, and M. Yoder, The Electrochemical Society, 89-12, 1989, 1-13.

4. Bolton, W. von, "Über Die Ausschiedung Von Kohlenstoff In Form A Von Diamant," Zeitscrift Für Electrochemie, 17, November 15, 1911, 971-2.

5. Angus, J. "History of Diamond Growth at Metastable Conditions," Proceedings of the First International Symposium on Diamond and Diamond-like Films, edited by Dismukes, J. P., A. J. Purdes, B. S. Meyerson, T. D. Moustakas, D. E. Spear, F. V. Ravi, and M. Yoder, The Electrochemical Society, 89-12, 1989, 1-13.

6. Kiffer, A. D., "Synthesis of Diamond Form Carbon Monoxide," Tonawanda Laboratories, Linde Air Products Company, June 6, 1956.

7. Bundy, F. P., H. T. Hall, H. M. Strong, R. H. Wentorf, "Man-Made Diamonds," Nature, 176, July 9, 1955, 51-4.

8. Derjaguin, B. V., D. V. Fedoseev, V. M Lukyanovich, B. V. Spitzin, V. A. Ryabov, and A. V. Lavrentyev, "Filamentary Diamond Crystals," Journal of Crystal Growth, 2, 1968, 380-4.

9. Lander, J. J. and J. Morrison, "Low Energy Diffraction Study of The {111} Diamond Surface," Surface Science, 4, 3, May-June 1966, 241-6.

10. Angus, John C., Herbert A. Will, and Wayne S. Stanko, "Growth of Diamond Seed Crystals By Vapor Deposition," Journal of Applied Physics, 39, 6, May 1968, 2915-22.

11. Bachmann, P. and R. Messier, "Emerging Technology of Diamond Thin Films," Chemistry and Engineering News, May 15, 1989, 24-39.

12. Deryagin, B. V. and D. V. Fedoseev, "Epitaxial Synthesis of Diamond In The Metastable Region," Russian Chemical Reviews, 39, 9, 1970, 783-8.

13. Bachmann, P. and R. Messier, "Emerging Technology of Diamond Thin Films," Chemistry and Engineering News, May 15 1989 pp. 24-39.

14. Johnson, W. L., III, "The Characterization Of Graphitic And Nongraphitic Carbon By Laser Raman Microprobe Analysis," in Microbeam Analysis edited by A. D. Romig Jr. and W. F. Chambers, San Francisco Press, Inc., 1986, 26-8.

15. Chang, C. P., D. L. Flamm, D. E. Ibbotson, and J. A. Mucha, "Diamond Crystal Growth By Plasma Chemical Vapor Deposition," Journal Of Applied Physics, 63, 5, March 1, 1988, 1744-8.

16. Knight, Diane S. and William B. White, "Characterization of Diamond Films By Raman Spectroscopy," Journal of Materials Science, 4, 2, March-April 1989, 385-93.

17. Williams, B. E., H. S. Kong, and J. T. Glass, "Electron Microscopy of Vapor Phase Deposited Diamond," Journal of Materials Research, 5, 4, April 1990, 801-10.

18. Pool, Robert, "Diamond Films Sparkle As They Come To Market," Science, 249, July 6, 1990, 27-8.

19. "Improving Perfection," The Economist, 316, 7663, July 14, 1990, 84.

20. Anthony, T. R., W. F. Banholzer, J. F. Fleischer, Lanhua Wei, P. K. Kuo, R. L. Thomas, and R. W. Pryor, "Thermal Diffusivity of Isotopically Enriched ^{12}C Diamond," Physical Review B, 42, 2, July 15, 1990, 1104-1111.

21. Suzuki, Kazuhiro, Atsuhito Sawabe, and Tadao Inuzuka, "Characterizations of The DC Discharge Plasma During Chemical Vapor Deposition For Diamond," Applied Physics Letters, 53, 19, November 7, 1988, 1818-9.

22. Joshi, Asawari, A. Gangal, and S. K. Kulkarni, "Structure and Properties of Diamondlike Carbon Coatings Deposited In RF Plasma From Benzene and Monosubstituted Benzenes," Journal of Applied Physics, 64, 12, December 15, 1988, 6668-72.

23. Williams , B. E. and J. T. Glass, "Characterization of Diamond Thin Films: Diamond Phase Identification, Surface Morphology, And Defect Structures," Journal of Materials Research, 4, 2, March-April, 1989, 373-84.

24. Kitahama, Katsuki, Kazuhiko Hirata, Hirohide Nakamatsu, Shichio Kawai, Naoji Fujimori, Takahiro Imai, Hiroshi Yoshino, and Akira Doi, "Synthesis Of Diamond By Laser-Induced Chemical Vapor Deposition," Applied Physics Letters, 49, 11, September 15, 1986, 634-5.

25. Kitahama, Katsuki, Kazuhiko Hirata, Hirohide Nakamatsu, Shichio Kawai, Naoji Fujimori, and Takahiro Imai, "Synthesis Of Diamond By Laser-Induced CVD, in *Photon, Beam, and Plasma Stimulated Chemical Processes At Surfaces*, Material Research Society Symposia, 75, 1987, 309-15.

26. Kitahama, Katsuki, "Reinvestigation of the Carbon Films Prepared By ArF Excimer Laser-Induced Chemical Vapor Deposition," Applied Physics Letters, 53,19, November 7, 1988, 1812-4.

27. Badzian, Andrzej R., and Robert C. DeVries, "Crystallization of Diamond From The Gas Phase; Part 1," Materials Research Bulletin, 23, 1988, 385-400.

28. Martin, L. Robbin and Michael W. Hill, "Methyl Regeneration: An Important Role For Hydrogen Atoms In Diamond Film Synthesis," in Proceedings of the First International Symposium on Diamond and Diamond-like Films, edited by Dismukes, J. P., A. J. Purdes, B. S. Meyerson, T. D. Moustakas, D. E. Spear, F. V. Ravi, and M. Yoder, The Electrochemical Society, 1989, 568-75.

29. Spear, Karl E., "Diamond-Ceramic Coating of The Future," Journal of The American Ceramic Society, 72, 2, 1989, 171-91.

30. Vandenbulcke, L., P. Bou, and G. Moreau, "On The Control Of Diamond Deposition Structure and Morphology," Proceedings of the First International Symposium on Diamond and Diamond-like Films, edited by Dismukes, J. P., A. J. Purdes, B. S. Meyerson, T. D. Moustakas, D. E. Spear, F. V. Ravi, and M. Yoder, The Electrochemical Society, 89-12, 1989, 594-609.

31. Badzian, Andrzej R., and Robert C. DeVries, "Crystallization of Diamond From The Gas Phase; Part 1," Materials Research Bulletin, 23, 1988, 385-400.

32. Badzian, Andrzej R., and Robert C. DeVries, "Crystallization of Diamond From The Gas Phase; Part 1," Materials Research Bulletin, 23, 1988, 385-400.

33. Pate, B. B., "The Diamond Surface: Atomic and Electronic Structure," Surface Science, 165, 1986, 83-142.

34. Joshi, A., "Oxidation Behavior of Carbon and Diamond Films," in Thermal Analysis of Metallurgical Systems, TMS, Warrendale, PA, 1990.

35. Herziger, Dr. Gerd, "The Influence of Laser-Induced Plasma On Laser Materials Processing," in The Industrial Laser Annual Handbook, 1986 Edition, edited by David Belforte and Morris Levitt, 1986, pages: 108-15.

36. Allen, S. D., J. A. Goldstone, J. P. Stone, and R. Y. Jan, "Transient Nonlinear Laser Heating and Deposition: A Comparison of Theory and Experiment," Journal of Applied Physics, 59, 5, March 1, 1986, 1653-7.

37. Perry, Robert H. and Don Green, Perry's Chemical Engineers' Handbook, Sixth Edition, McGraw-Hill, 1984.

38. Bauerle, Dieter, Chemical Processing With Lasers, Springer-Verlag, 1986.

39. Allen, S. D., R. Y. Jan, S. M. Mazuk, and S. D. Vernon, "Real Time Measurement Of Deposition Initiation And Rate In Laser Chemical Vapor Deposition," Journal Of Applied Physics, 58, 1, July 1, 1985, pages: 327-31.

40. Bauerle, Dieter, Chemical Processing With Lasers, Springer-Verlag, 1986.

41. Copley, Stephen M., "Mass Transport During Laser Chemical Vapor Deposition," Journal of Applied Physics, 64, 4, August 15, 1988, 2064-8.

42. Kobayashi, H., M. Shen, and A. T. Bell, "The Role Of Halogens In The Plasma Polymerization Of Hydrocarbons," Journal Of Macromolecular Science-Chemistry, A8(8), 1974, pages: 1345-60.

43. Yasuda, H., Plasma Polymerization, Academic Press, 1985.

44. Kline, Laurence E., William D. Partlow, and William E. Bies, Electron and Chemical Kinetics In Methane RF Glow-Discharge Deposition Plasmas, Journal Of Applied Physics, 65, 1, January 1989, 70-9.

45. Johnson, N. P., A. P. Webb, and D. J. Fabian, "A Mass Spectrometric System For The Study Of Transient Plasma Species In Thin Film Deposition," Material Research Society Symposia Proceedings, Volume 30, 1984, Elsevier Science Publishing, 277-82.

46. Kline, Laurence E., William D. Partlow, and William E. Bies, "Electron and Chemical Kinetics In Methane RF Glow-Discharge Deposition Plasmas," Journal of Applied Physics, 65, 1, January 1989, 70-7.

47. Tachibana, K., M. Nishida, H. Harima, and Y. Urano, "Diagnostics and Modelling Of A Methane Plasma Used In The Chemical Vapour Deposition Of Amorphous Carbon," Journal of Physics D: Applied Physics, 17, 1984, 1727-42.

48. Suzuki, Kazuhiro, Atsuhito Sawabe, and Tadao Inuzuka, "Characterizations of The DC Discharge Plasma During Chemical Vapor Deposition For Diamond," *Applied Physics Letters*, 53, 19, November 7, 1988, 1818-9.

49. Inspektor, A., T. McKenna, Y. Liou, L. Bourget, K. E. Spear, and R. Messier, "Plasma Chemistry In Diamond Deposition," in Proceedings Of The First International Symposium On Diamond and Diamond-Like Films, edited by J. P. Dismukes, A. J. Purdes, B. S. Meyerson, T. D. Moustakes, K. E. Spear, D. V. Ravi, and M. Yoder; The Electrochemical Society Proceedings Volume 89-12, 1989, 342-52.

50. Roman, Ward C., Meredith B. Colket III, Stephen O. Hay, and Alan C. Eckbreth, " CARS Diagnostics and Analysis of Species In Diamond Deposition Process," in Proceedings Of The First International Symposium On Diamond and Diamond-Like Films, edited by J. P. Dismukes, A. J. Purdes, B. S. Meyerson, T. D. Moustakes, K. E. Spear, D. V. Ravi, and M. Yoder; The Electrochemical Society Proceedings Volume 89-12, 1989, 330-41.

51. Hargis, P. J., Jr., and K. E. Greenberg, "Pulsed-Ultraviolet Laser Raman Diagnostics Of Plasma Processing Discharges," Applied Physics Letters, 53, 19, November 7, 1988, 1809-11.

52. Butler, James E. and Francis G. Celii, "Vapor Phase Diagnostics In CVD Diamond Deposition," in Proceedings Of The First International Symposium On Diamond and Diamond-Like Films, edited by J. P. Dismukes, A. J. Purdes, B. S. Meyerson, T. D. Moustakes, K. E. Spear, D. V. Ravi, and M. Yoder; The Electrochemical Society Proceedings Volume 89-12, 1989, 317-29.

53. Miller, John C. and Charles S. Feigerle, "Multiphoton Ionization of Transient Species In Supersonic Jets," Resonance Enhanced Spectroscopy 1988, April 1988, 101.

54. Tsai, Bilin P., Russell D. Johnson III, and Jeffrey W. Hudgens, "Resonance Enhanced Multiphoton Ionization Spectroscopy of 2-Butene-1-yl (C_4H_7) Between 455-485 nm," Resonance Enhanced Spectroscopy 1988, April 1988, 129-132.

55. Meier, W., H. Rottke, and H. Zacharias, "State Selective Ionization of Molecular Hydrogen," Resonance Enhanced Spectroscopy 1988, April 1988, 93-9.

56. Hessler, Jan P. and Wallace L. Glab, "Two-Color, Doppler-Free Ionization of Molecular Hydrogen For Isotopic Analysis," Resonance Enhanced Spectroscopy 1988, April 1988, 183-7.

57. Sultan, G. and G. Baravian, "Resonant Multiphoton Ionization Cross-Sections. Application To CO," Resonance Enhanced Spectroscopy 1988, April 1988, 339-40.

58. Wiley, W. C. and I. H. McLaren, "Time-of-Flight Mass Spectrometer With Improved Resolution," The Review Of Scientific Instruments, 26, 12, December 1955, 1150-7.

59. Hudgens, Jeffrey W., "Progress In Resonance Enhanced Multiphoton Ionization Spectroscopy of Transient Free Radicals," Advances in Multi-photon Processes and Spectroscopy, Volume 4, edited by S. H. Lin, Singapore: World Scientific, 1988.

60. Ohtake, Naoto, Hitoshi Tokura, Yasuhiko Kuriyama, "Synthesis of Diamond Film By Arc Discharge Plasma CVD," Proceedings of the First International Symposium on Diamond and Diamond-like Films, edited by Dismukes, J. P., A. J. Purdes, B. S. Meyerson, T. D. Moustakas, D. E. Spear, F. V. Ravi, and M. Yoder, The Electrochemical Society, 89-12, 1989, 93-105.